ELSEVIER

Physica D 173 (2002) 204–225

PHYSICA D

www.elsevier.com/locate/physd

The Hamiltonian perturbation approach of two interacting nonlinear waves or solitary pulses in an optical coupler

Yannis Kominis, Kyriakos Hizanidis*

Department of Electrical and Computer Engineering, National Technical University of Athens, 9 Iroon Polytexniou, 157 73 Athens, Greece

Received 31 August 2001; received in revised form 19 April 2002; accepted 31 May 2002
Communicated by I. Gabitov

Abstract

The traveling-wave solutions dynamics of two linearly coupled nonlinear Schrödinger equations, describing the wave propagation in a dual-core optical fiber, is studied in the framework of the Hamiltonian perturbation theory. The surface of section of the phase space for each wave is obtained as a contour plot of an approximate invariant of the system and the phase space distortions due to the interaction are analyzed. Depending on the magnitude of the coupling strength, the parametric resonance involved leads to weak, strong and chaotic interactions. The coupling strength threshold above which the interaction between two nonlinear waves of given amplitude becomes chaotic is also estimated. On the other hand, the interaction of a solitary pulse with a nonlinear periodic wave is studied using the Melnikov method for homoclinic orbits. This interaction causes stochastization of the homoclinic orbit, which corresponds to the solitary pulse and the separatrix splitting as well as the width of the stochastic layer near this orbit is given in terms of the Melnikov function. The latter is applied in the case of two interacting solitary pulses as well.

PACS: 05.45.−a; 41.20.−q; 42.65.Wi; 42.81.−i; 43.20.+g

1. Introduction

The last few years there has been a considerable amount of research work as well as experiments on designing high-bit-rate fiber systems based on solitary pulses. Soliton communication systems are expected to be commercially available in a few years, operating at Tbit data rates. However, the success of these systems is highly dependent on the development of devices capable for fast operations in the optical layer, as exchange of information between different channels, satisfying the demand for an all-optical switching. A key physical mechanism governing these processes is the coupling between two nonlinear waves or pulses.

The nonlinear coupler is a two-core device extensively studied for its potential applications in optical communication systems [1–12]. The coupling between the two waves is a result of the overlap between the evanescent tails of the fields of the two-cores, which is considered as a relatively weak perturbation with respect to the uncoupled

* Corresponding author. Fax: +30-1-772-3513.
E-mail address: kyriakos@central.ntua.gr (K. Hizanidis).

0167-2789/02/$ – see front matter
PII: S0167-2789(02)00551-1

propagation that is governed by a single nonlinear Schrödinger equation (NLSE). The coupling coefficient is assumed to be reasonably constant over the frequency spectrum of the coupled wave fields [2]. The system of two linearly coupled nonlinear Schrödinger equation (LCNLSE) governing the wave propagation in the two-cores is mostly studied from a quasi-particle point of view. The latter involves the perturbation methods, applied on an ansatz of the pulse with a specific time profile (hyperbolic secant or Gaussian), which yield respective evolution (with pulse propagation) equations for the pulse width, amplitude or any other parameter entering in the ansatz [3–5]. Numerical studies of the LCNLSE, investigating the propagation of NLSE solitons have also been reported [6–9].

In this paper we investigate the dynamics of the stationary or traveling (depending on the choice of the frame of reference) wave solutions of the LCNLSE. In order to understand the importance of the stationary solutions we first consider a single NLSE which defines a Hamiltonian dynamical system on an infinite-dimensional space of a complex function. As it is known, the behavior of the solutions is defined to a large extent, by the singular points of the system (i.e. the stationary solutions) and depends strongly on the nature of these points (as determined by the stability of its stationary solutions). The dynamics of the system can be explained in the context of a quasi-periodic evolution in two dimensions, namely time t and propagation distance ξ. The time profile of the solution as described by the stationary solutions can be constant, periodic or asymptotic corresponding to a continuous wave, a nonlinear periodic wave or a solitary pulse (which is actually a limiting case of a nonlinear periodic wave), respectively. Propagation of a time profile can also be constant, periodic or asymptotic with respect to the propagation distance. Combinations of these kinds of evolutions in both dimensions lead to the formation of: stationary periodic solutions (τ: periodic, ξ: constant), quasi-periodic solutions (τ: periodic, ξ: periodic), solitons with zero asymptote (τ: asymptotic, ξ: constant), solitons with nonzero asymptotes (τ: asymptotic, ξ: periodic), rational solitons (τ: asymptotic, ξ: asymptotic) and modulationaly instable modes (τ: almost constant, ξ: periodic or asymptotic). All the solutions have been studied analytically [13] as well as numerically while the numerical simulation of quasi-periodic solutions has very interesting features associated with numerically induced chaos [14].

The introduction of sufficiently small linear coupling in the case of two weakly LCNLS, acts like a Hamiltonian perturbation on the aforementioned integrable system. Since the NLS is structurally stable under Hamiltonian perturbations the qualitative features of system dynamics persist. However, the stationary solutions change proportionally to the actual perturbation strength resulting in periodic solutions with varying amplitude and wavy-shaped asymptotic solutions. This is analogous to the displacement of the fixed points of a finite dimensional system under perturbation. Moreover, under stronger perturbation (i.e. stronger coupling) the stationary solutions can be chaotic in the usual Hamiltonian sense, resulting in a complex irregular evolution during propagation.

The stationary solutions of the LCNLS are associated with Hamiltonian system of two degrees of freedom; namely that of the system of two coupled Duffing oscillators (CDO). Since this system is nonintegrable for nonzero coupling coefficient, there are two approaches that can be followed for studying its dynamics: the first one is the searching for special solutions existing in restricted areas of the phase and parameter space of the system [15]. This method has already given some special asymptotic solutions corresponding to solitary pulses, but it gives no information about the structure of the entire phase space of the system. In the second one, which is followed in this work, the CCO system is considered as a perturbation of an integrable one, namely the two uncoupled Duffing oscillators. This perturbation, due to the interaction between two waves or pulses, possesses all the characteristics that are well-known to occur in coupled nonlinear oscillators, namely interlaced phase space regions of regular and chaotic dynamics [16–19].

The nonlinear periodic waves described by the NLSE have amplitude dependent frequency and are characterized by the presence of higher harmonics of the fundamental frequency in their spectrum. Consequently, a nonlinear periodic wave in one fiber affects mostly nonlinear periodic waves of specific amplitude and frequency of the other fiber due to resonance between harmonics of the two waves. Sufficiently far from an exact resonance, the interactions can be described by two approximate invariants of the nonintegrable Hamiltonian system, the contour plots of which provide the Poincare surface of section for each degree of freedom with satisfactory accuracy [16]. The interaction

of two waves with commensurable or almost commensurable frequencies is more drastic in the sense that the phase space is highly distorted in the neighborhood of an exact resonance compared to the uncoupled case. The strength of a resonant interaction (associated with the respective resonance width) depends not only on the coupling strength but also on the pair of interacting waves through the amplitude of the harmonic of each wave that satisfy the given resonant condition. Under increasing coupling strength the interaction does not only modify but actually destructs the (uncoupled) nonlinear periodic waves. This effect is described by the overlapping of adjacent resonances in the phase space since the width of each resonance increases with coupling strength, and a criterion for destructive wave interaction can then be established [17].

The interaction of a solitary pulse in one of the fibers with a nonlinear periodic wave in the other has all the typical characteristics of the modification of a homoclinic orbit under the influence of an external driving force [18,19]. One of these typical characteristics is the presence of homoclinic points where the stable and unstable manifolds intersect transversely instead of joining smoothly as if there was no coupling. This transverse intersection of the two manifolds is a condition (sufficient for the formation of a stochastic layer near the homoclinic orbit) where the dynamics can be described by the well-known "horse-shoe" map [19]. The distortion of the homoclinic orbit associated with a solitary pulse due to each coupling with the nonlinear wave as well as the width of the stochastic layer are described in terms of the Melnikov method [18,19]. Since the soliton pulse is the limiting case of two one-parameter families of nonlinear periodic waves, the interaction of two such pulses can also be studied in the context of Melnikov method as a nonlinear periodic wave with infinite period.

This work is organized as follows. In Section 2 the equations modeling the wave propagation in the dual-core are provided. In Section 3 the nonlinear periodic wave interactions are described. The construction of the approximate invariants for the nonresonant interactions is included in Section 3.1, while the width of each resonance is estimated in Section 3.2. A criterion for the destruction of the uncoupled nonlinear periodical waves under coupling is presented in Section 4. Section 5 contains the derivation of the Melnikov's function describing the splitting of the two manifolds that form the aforementioned homoclinic orbit under the influence of a nonlinear periodic wave or a pulse propagating in the other fiber. Finally, in Section 6, the main conclusions of this work are evaluated and summarized.

2. The physical model

The propagation of two coherent waves in a nonlinear dual-core fiber, for the case of similar cores, can be described in terms of two linearly coupled NLSEs. In normalized (soliton) units this set of coupled NLSEs is given by

$$i\frac{\partial U}{\partial \xi}+\frac{1}{2}\frac{\partial^2 U}{\partial \tau^2}+|U|^2U+KV=0, \qquad i\frac{\partial V}{\partial \xi}+\frac{1}{2}\frac{\partial^2 V}{\partial \tau^2}+|V|^2V+KU=0. \tag{1}$$

Here, $U(\xi,\tau)$ and $V(\xi,\tau)$ are envelope functions and K is the normalized coupling coefficient between the two-cores. We examine the dynamics of solutions of the form

$$U(\xi,\tau)=u(\tau)\exp(iq\xi), \qquad V(\xi,\tau)=v(\tau)\exp(iq\xi), \tag{2}$$

where the amplitudes $u(\tau)$, $v(\tau)$ are real functions of τ and q is a real parameter of the solution.

Concerning the form of the solutions in hand, two things should be mentioned. The first is that we restrict ourselves to the study of 'coherent' waves, meaning that the parameter q is identical for the waves propagating in both cores. And the second is that if Eq. (2) is a solution of Eq. (1), then the traveling-wave solution

$$U'(\xi,\tau)=u(\tau-c\xi)\exp\left(ic\tau+i\left(\frac{q-c^2}{2}\right)\xi\right), \qquad V'(\xi,\tau)=v(\tau-c\xi)\exp\left(ic\tau+i\left(\frac{q-c^2}{2}\right)\xi\right). \tag{3}$$

Also satisfies Eq. (1) (manifestation of the well-known Galilean invariance). After substituting Eq. (2) in the coupled NLSEs the following system of two real ordinary differential equations is obtained

$$\frac{1}{2}\frac{\mathrm{d}^2u}{\mathrm{d}\tau^2} - qu + u^3 + Kv = 0, \qquad \frac{1}{2}\frac{\mathrm{d}^2v}{\mathrm{d}\tau^2} - qv + v^3 + Ku = 0. \tag{4}$$

This system can also be described, in the framework of the Hamiltonian dynamics, as a system of two degrees of freedom via the Hamiltonian function

$$H(u, v, \dot{u}, \dot{v}) = \left(\frac{\dot{u}^2}{2} - qu^2 + \frac{u^4}{2}\right) + \left(\frac{\dot{v}^2}{2} - qv^2 + \frac{v^4}{2}\right) + 2Kuv. \tag{5}$$

Here the dot denotes the derivatives with respect to τ.

Using the scale transformation for the functions and variables involved

$$u = \sqrt{|q|}x, \quad v = \sqrt{|q|}y, \quad \tau = \sqrt{2|q|}t, \quad H = 2q^2\bar{H}, \quad \varepsilon = \frac{K}{q}, \tag{6}$$

the Hamiltonian function is transformed into the following form:

$$\bar{H}(x, y, \dot{x}, \dot{y}) = \left(\frac{\dot{x}^2}{2} - \mathrm{sgn}(q)\frac{x^2}{2} + \frac{x^4}{4}\right) + \left(\frac{\dot{y}^2}{2} - \mathrm{sgn}(q)\frac{y^2}{2} + \frac{y^4}{4}\right) + \varepsilon xy. \tag{7}$$

This Hamiltonian can be decomposed as follows (from now on the bar on H is omitted for simplicity of the notation)

$$H = H_{0x} + H_{0y} + \varepsilon H_1, \quad H_{0x} = \left(\frac{\dot{x}^2}{2} - \mathrm{sgn}(q)\frac{x^2}{2} + \frac{x^4}{4}\right),$$
$$H_{0y} = \left(\frac{\dot{y}^2}{2} - \mathrm{sgn}(q)\frac{y^2}{2} + \frac{y^4}{4}\right), \quad H_1 = xy. \tag{8}$$

In this decomposition, Eq. (8), H_{0x} and H_{0y} describe the wave propagation in each core in the absence of the other while H_1 describes the coupling between them. It is worth noticing that the perturbation term H_1 is proportional to $\varepsilon = K/q$ which plays the role of the so-called "small parameter" in this analysis. However, generally speaking the results of the latter are not restricted solely to the case of a small coupling coefficient K.

The system of two degrees of freedom described by the Hamiltonian (Eq. (8)) is known to be nonintegrable for $\varepsilon \neq 0$, as there is no known additional constant of the motion apart from the Hamiltonian function itself. Following the usual technique for nonintegrable Hamiltonian systems, the dynamical behavior of the system in hand will be studied by perturbing the respective integrable one. The latter is the one describing the dynamics of two uncoupled nonlinear oscillators with the Hamiltonian function being

$$H = H_{0x} + H_{0y}. \tag{9}$$

Here, H_{0x} and H_{0y} are the two constants of the motion necessary for integrability, representing the generalized energy of each oscillator.

Before proceeding to the analysis of the near-integrable system (Eq. (8)) it is necessary to refer to some concepts of the dynamics of the unperturbed system (Eq. (9)). This system can be considered as one, which is embedded in the phase space of a dynamical system of two degrees of freedom. We restrict our description in the dynamics of one of the oscillators, described by the Hamiltonian function. However, what follows is valid also for the second oscillator since they are identical and uncoupled. In Appendix A, the dynamics of the unperturbed system, the solutions, their respective Fourier expansions as well as their transformation to action-angle variables are given. The transformation to action-angle variables is necessary for the perturbation methods which are utilized in the next sections in order to

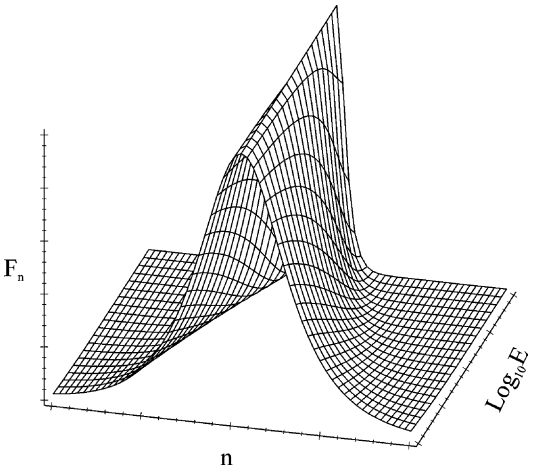

Fig. 1. Linear spectrum of a nonlinear periodic wave.

study the dynamics of the actual near-integrable perturbed system. It must be emphasized that the oscillating solutions given by Eqs. (A.3) and (A.4) possess the main characteristics of the nonlinear motion, namely: (a) the period depends on the generalized energy; (b) the linear spectrum contains more than one frequencies (nonharmonicity).

In (J, θ) variables the Hamiltonian of the unperturbed system can be written in the form

$$H_0 = H_{0x}(J_x) + H_{0y}(J_y), \qquad \theta_x = \omega_x t + \theta_{0x}, \qquad \theta_y = \omega_y t + \theta_{0y}, \tag{10}$$

where ω_x, ω_y are the angular frequencies of the x and y oscillations, respectively. From now on we can use (J_x, J_y) instead of (E_x, E_y) as the two integrals of the motion of the unperturbed system when it is useful.

It is important for the following analysis to note that the Fourier coefficients (F_n) of the series, Eqs. (A.12) and (A.13), are decreasing with $|n|$ hyperbolic secant functions. Furthermore, the width of this function broadens as the generalized energy of the oscillation approaches the value $E_x = 0$, as shown in Fig. 1. When the energy approaches zero the distance between subsequent harmonics in the linear spectrum approaches zero, the spectrum tends to be continue (nonperiodic solution) and its width increases since it is proportional to the solution period. Therefore, as the value of the generalized energy approaches zero (and the period becomes infinite), the nonlinear oscillatory solutions can be represented satisfactorily by their Fourier series if one keeps retaining a continuously increasing number of terms.

3. Interactions between nonlinear periodic waves

In this section, the coupling of the nonlinear periodic oscillations mentioned previously is examined. Under the Galilean transformation these oscillations correspond to nonlinear periodic waves propagating in each core.

It is obvious that, depending upon the oscillation energy of each degree of freedom (E_x, E_y), three different pairs of oscillations that may be coupled can be obtained. According to the kind of the Jacobi elliptic function that represents each oscillation one has the following cases:

- Case A ($E_x > 0$, $E_y > 0$): cnoidal–cnoidal interaction.
- Case B ($-1/4 < E_x < 0$, $-1/4 < E_y < 0$): dnoidal–dnoidal interaction.
- Case C ($E_x > 0$, $-1/4 < E_y < 0$): cnoidal–dnoidal interaction.

The method used in order to study the dynamics of the near-integrable Hamiltonian system (Eq. (8)) is the canonical perturbation method, which is very popular in the context of classical mechanics [16]. According to the famous KAM theorem, an integrable Hamiltonian system (with Hamiltonian H_0) preserves the regularity of many of its orbits under a perturbation which renders it to a near-integrable one (with Hamiltonian $H = H_0 + H_1$). The orbits that are preserved, although slightly modified, are those which correspond to initial conditions which would result to nonresonant orbits of the unperturbed system; it is then necessary the ratio of the unperturbed frequencies to be an irrational number. For these orbits an approximate local additional integral of the motion (apart from the Hamiltonian which is an integral of the motion since it is time-independent) can be constructed with the use of canonical perturbation theory leading to locally 'organized' motion. The topology of the resonant orbits of the unperturbed system corresponding to rational ratio of unperturbed frequencies is destroyed under perturbation leading to complex local dynamics. The strong violation of the unperturbed topology for these orbits under perturbation manifests itself as a divergence of the constructed local integral of the motion due to small denominators. It is important for understanding the complete dynamics of the system to keep in mind that the resonant orbits are dense in phase space (exactly as dense as the set of rational numbers in the set of real numbers). However, not all of these resonances modify the phase space topology at the same extent, so on one can distinguish between more and less important resonances (in commonly used terminology, resonances of different orders). Also the extent of all resonances depends on the strength of the perturbation.

3.1. Nonresonant interaction

After transforming to action-angle variables the Hamiltonian, Eq. (8), takes the form

$$H(\mathbf{J}, \boldsymbol{\theta}) = H_0(\mathbf{J}) + \varepsilon H_1(\mathbf{J}, \boldsymbol{\theta}), \tag{11}$$

where bold letters are used to denote vectors

$$H_0(\mathbf{J}) = H_{0x}(J_x) + H_{0y}(J_y), \tag{12}$$

and H_1 is a multi-periodic function of the angles

$$H_1 = \sum_m H_{1m}(\mathbf{J}) \exp(i\mathbf{m} \cdot \boldsymbol{\theta}), \tag{13}$$

with

$$\mathbf{m} \cdot \boldsymbol{\theta} = m_1\theta_1 + m_2\theta_2. \tag{14}$$

The transformation to new variables $(\bar{J}_x, \bar{J}_y, \bar{\theta}_x, \bar{\theta}_y)$ (for which the new Hamiltonian $\bar{H}$ is a function of the new actions alone) by utilizing a near-identity generating function $S(\bar{\mathbf{J}}, \boldsymbol{\theta})$ and expanding S and $\bar{H}$ in power series in ε yields to zero order

$$\bar{H}_0(\bar{\mathbf{J}}) = H_0(\bar{\mathbf{J}}), \tag{15}$$

while, to first order

$$\bar{H}_1 = \boldsymbol{\omega}(\mathbf{J}) \cdot \frac{\partial S_1(\bar{\mathbf{J}}, \bar{\boldsymbol{\theta}})}{\partial \bar{\boldsymbol{\theta}}} + H_1(\bar{\mathbf{J}}, \bar{\boldsymbol{\theta}}), \tag{16}$$

with

$$\boldsymbol{\omega}(\bar{\mathbf{J}}) = \frac{\partial H_0(\bar{\mathbf{J}})}{\partial \bar{\mathbf{J}}}, \tag{17}$$

being the frequency vector of the unperturbed motion.

Following the standard procedure of averaging over all the angle variables yields

$$\bar{H} = H_0(\bar{\mathbf{J}}) + \varepsilon \left\langle H_1(\bar{\mathbf{J}}, \bar{\boldsymbol{\theta}}) \right\rangle, \tag{18}$$

and

$$\boldsymbol{\omega} \cdot \frac{\partial S_1}{\partial \boldsymbol{\theta}} = -\{H_1\}, \tag{19}$$

where $\langle\rangle$ and $\{\}$ denote the average and the oscillating part of H_1, respectively.

The averaged Hamiltonian $\bar{H}$ is a function of $\bar{\mathbf{J}}$ only and thus one can obtain the first order correction of the unperturbed frequencies due to the coupling

$$\Delta\boldsymbol{\omega} = \varepsilon \frac{\partial \left\langle H_1(\bar{\mathbf{J}}, \bar{\boldsymbol{\theta}}) \right\rangle}{\partial \bar{\mathbf{J}}}. \tag{20}$$

Solving Eq. (19) for S_1 and inserting the solution to the transformation equations the following new approximate constants of the motion of the perturbed system $\bar{\mathbf{J}}$ are obtained

$$\bar{J}_x = J_x - \varepsilon \frac{\partial S_1}{\partial \theta_\chi}, \tag{21}$$

$$\bar{J}_y = J_y - \varepsilon \frac{\partial S_1}{\partial \theta_y}. \tag{22}$$

By setting $\theta_y = \textit{constant}$ the Poincare surface of section (J_x, θ_x) for different values of J_y and perturbation strength ε can be constructed. The expressions Eqs. (21) and (22) can also be used to obtain the new (modified) constant generalized energies of the two degrees of freedom since actions and generalized energies are connected through Eqs. (A.8) and (A.9). It is important to remark that the variance of the actions expressed by the term proportional to ε in (21), (22) is a measure of the energy coupling between the two degrees of freedom. This energy coupling obviously depends on the coupling (perturbation) strength but also on the specific values of the energies of the coupled oscillations as it can be seen from the dependence of S_1 on the energies of the two degrees of freedom. For practical reasons we can plot the 'surface of section' (E_x, θ_x) although E_x and θ_x are not canonically conjugate variables, however the qualitative results remain the same. After substituting the Fourier expansions for x and y in the perturbed Hamiltonian and following the procedure previously described the results for each one of the three cases.

Case A. The Hamiltonian in this case is

$$H = H_{0x}(J_x) + H_{0y}(J_y) + \varepsilon \sum_{n_x,n_y=1}^{\infty} H_{n_x,n_y}(J_x, J_y) \times\{\cos[(2n_x - 1)\theta_x + (2n_y - 1)\theta_y] + \cos[(2n_x - 1)\theta_x - (2n_y - 1)\theta_y]\}, \tag{23}$$

where

$$H_{n_x,n_y}(J_x, J_y) = H_{n_x,n_y}(J_x(E_x), J_y(E_y)) = F_A(E_x, E_y) A_{n_x}(E_x) A_{n_y}(E_y), \tag{24}$$

$$F_A(E_x, E_y) = \sqrt{(1 + \sqrt{1 + 4E_x})(1 + \sqrt{1 + 4E_y})} \frac{\pi^2}{2 r_x r_y K(r_x) K(r_y)}, \tag{25}$$

$$A_{n_x}(E_x) = \operatorname{sec} h \left[\left(n_x - \frac{1}{2} \right) \pi \frac{K'(r_x)}{K(r_x)} \right], \tag{26}$$

$$A_{n_y}(E_y) = \operatorname{sec} h \left[\left(n_y - \frac{1}{2} \right) \pi \frac{K'(r_y)}{K(r_y)} \right]. \tag{27}$$

The first order frequency change due to coupling, on the other hand, is

$$\Delta\omega_x = \Delta\omega_y = 0, \tag{28}$$

while the two constants (to first order) of the motion are shown in Appendix B. Both x and y oscillations are symmetric about zero so that no averaging part in H_1 exist to modify the frequency to first order. This means that the distance between the maxima and minima of the coupled cnoidal waves is the same as if the waves were uncoupled.

Choosing a specific nonlinear y-wave in terms of an E_y value and a coupling strength in terms of ε, after setting $\theta_y = 0$ in $\bar{J}_x$ given by Eq. (B.1), a function $\bar{J}_x = \bar{J}_x(E_x, \theta_x)$ is obtained. The contour plot of this function yields the (E_x, θ_x)-surface of section in the phase space. For $\varepsilon = 10^{-3}$, $E_y = 1$ the function $\bar{J}_x = \bar{J}_x(E_x, \theta_x)$ and the corresponding (E_x, θ_x)-surface are shown in Fig. 2a and b, respectively. Since E_y is far from zero and the coupling strength is small, only the first harmonic of the y-wave seems to affect significantly the x-waves through a $(\omega_x = \omega_y)$-resonance, and only the area around $E_x = 1$ is distorted due to coupling. The effect of increasing the coupling strength to $\varepsilon = 10^{-2}$ is shown in Fig. 3a and b for the area around the $(\omega_x = \omega_y)$-resonance. If one magnifies the region near $E_x = 0$ we can see that the $(3\omega_x = \omega_y)$-resonance becomes visible (Fig. 3c and d). In Fig. 4a and b the case for $\varepsilon = 10^{-1}$ and $E_y = 10^{-2}$ is shown: the areas around $E_x = 1.7$ and $E_x = 11.4$ are highly affected by the y-wave through a $(\omega_x = 3\omega_y)$- and $(\omega_x = 5\omega_y)$-resonance, respectively.

It must be emphasized that the variation of the generalized energy is connected to the variation in action through the relation $\Delta E_x = \omega_x(E_x)\Delta J_x$. This explains why the $(\omega_x = 5\omega_y)$-resonance appears to be more significant than the $(\omega_x = 3\omega_y)$ one, while the $(\omega_x = \omega_y)$-resonance does not appear at all in the (E_x, θ_x)-surface of section. On the contrary that could not be the case if one have used the (J_x, θ_x)-surface of section instead.

Case B. Here, the Hamiltonian is

$$H = H_{0x}(J_x) + H_{0y}(J_y) + \varepsilon \sum_{n_x,n_y=0}^{\infty} H_{n_x n_y}(E_x, E_y)[\cos(n_x\theta_x + n_y\theta_y) + \cos(n_x\theta_x - n_y\theta_y)], \tag{29}$$

where

$$H_{n_x,n_y}(J_x(E_x), J_y(E_y)) = \begin{cases} \frac{1}{4}F_B(E_x, E_y), & n_x = n_y = 0, \\ \frac{1}{2}F_B(E_x, E_y)A_{n_x}(E_x), & n_x > 0, n_y = 0, \\ \frac{1}{2}F_B(E_x, E_y)A_{n_y}(E_y), & n_x = 0, n_y > 0, \\ F_B(E_x, E_y)A_{n_x}(E_x)A_{n_y}(E_y), & n_x > 0, n_y > 0, \end{cases} \tag{30}$$

$$F_B(E_x, E_y) = \sqrt{(1+\sqrt{1+4E_x})(1+\sqrt{1+4E_y})}\,\frac{\pi^2}{2K(q_x)K(q_y)}, \tag{31}$$

$$A_{n_x}(E_x) = \operatorname{sec} h\left(n_x\pi\frac{K'(q_x)}{K(q_x)}\right), \tag{32}$$

$$A_{n_y}(E_y) = \operatorname{sec} h\left(n_y\pi\frac{K'(q_y)}{K(q_y)}\right). \tag{33}$$

The frequency change to first order due to coupling becomes in this case

$$\frac{\Delta\omega_\chi}{\omega_\chi} = \frac{\varepsilon}{2}\frac{\partial F_B(E_x, E_y)}{\partial E_x}, \tag{34}$$

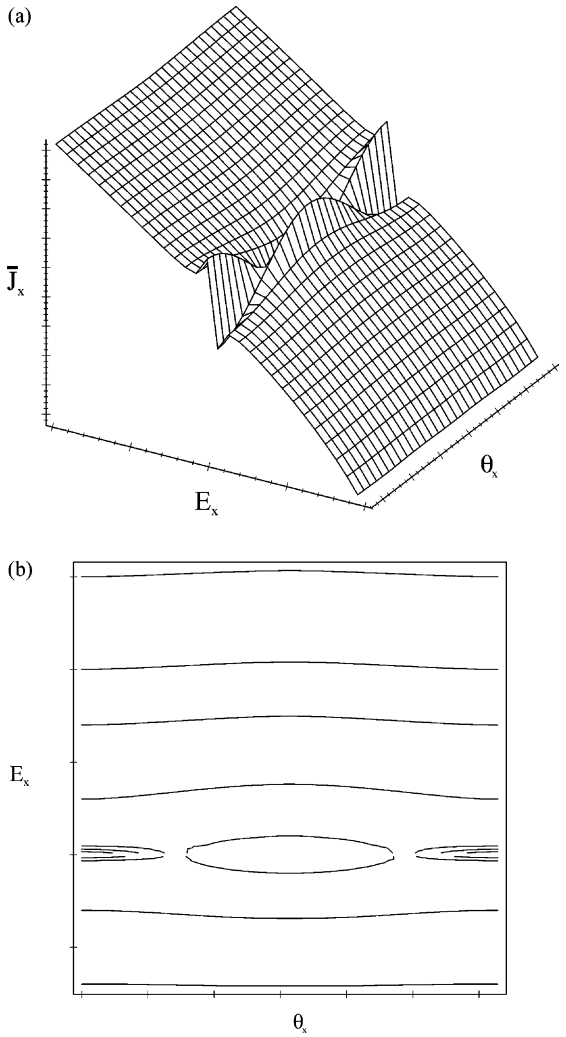

Fig. 2. (a) The function $\bar{J}_x = \bar{J}_x(E_x, \theta_x)$ and (b) the corresponding (E_x, θ_x)-surface of section with the $(\omega_x = \omega_y)$-resonance, for at $\varepsilon = 10^{-3}$ and $E_y = 1$.

$$\frac{\Delta\omega_y}{\omega_y} = \frac{\varepsilon}{2}\frac{\partial F_{\mathrm{B}}(E_x, E_y)}{\partial E_y}, \tag{35}$$

while the two first order constants of the motion are shown in Appendix B.

The modification of the frequency due to coupling is a very useful information for applications especially when requires the position in space (z) and time (τ) of the maximum value of the amplitude for each wave. This is the case in nonlinear couplers where, usually, the length of the coupler is designed so that the maximum amplitude is attainable at the end point. Following a similar procedure as in the Case A, we obtain the (E_x, θ_x)-surface of section for the coupling of the x-wave with an almost-harmonic y-wave of energy $E_y = -0.24$ under a coupling strength $\varepsilon = 10^{-2}$, as shown in Fig. 5a. In Fig. 5b, on the other hand, the (E_x, θ_x)-surface of section is shown for

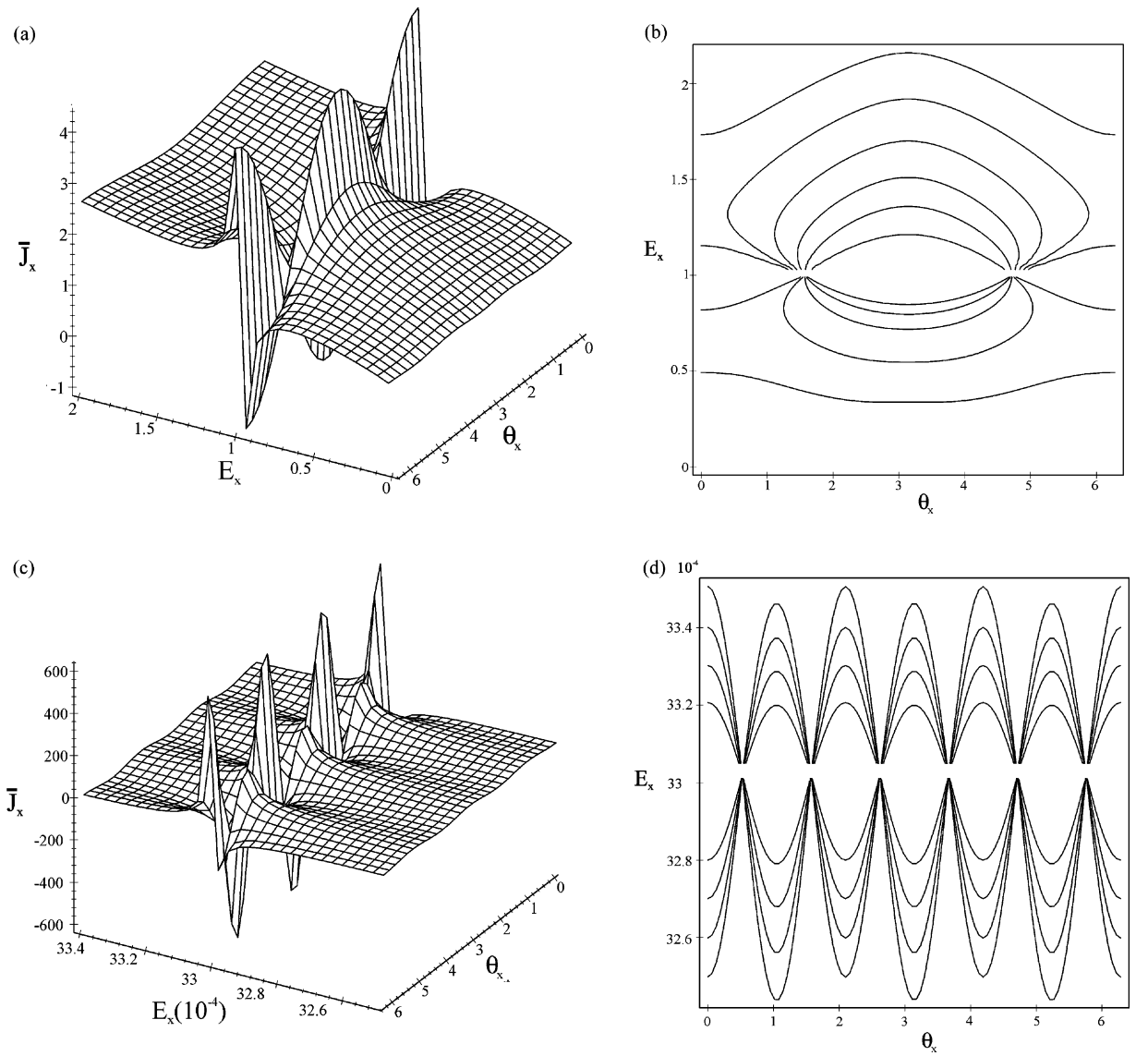

Fig. 3. (a) The function $\bar{J}_x = \bar{J}_x(E_x, \theta_x)$, (b) the corresponding (E_x, θ_x)-surface of section with the $(\omega_x = \omega_y)$-resonance and their respective magnifications (c) and (d) where the $(3\omega_x = \omega_y)$-resonance is visible near $E_x = 0$. Here $\varepsilon = 10^{-2}$ and $E_y = 1$.

the case of a quite nonharmonic y-wave of generalized energy $E_y = 10^{-4}$ with $\varepsilon = 10^{-2}$, where $E_x = -0.044$ and $E_x = -0.005$ correspond to $(\omega_x = 2\omega_y)$- and $(2\omega_x = 3\omega_y)$-resonance, respectively.

Case C. The Hamiltonian in this final case is

$$H = H_{0x}(J_x) + H_{0y}(J_y) + \varepsilon \sum_{n_x=1, n_y=0}^{\infty} H_{n_x,n_y}(E_x, E_y) \times [\cos((2n_x - 1)\theta_x + n_y\theta_y) + \cos((2n_x - 1)\theta_x - n_y\theta_y)], \tag{36}$$

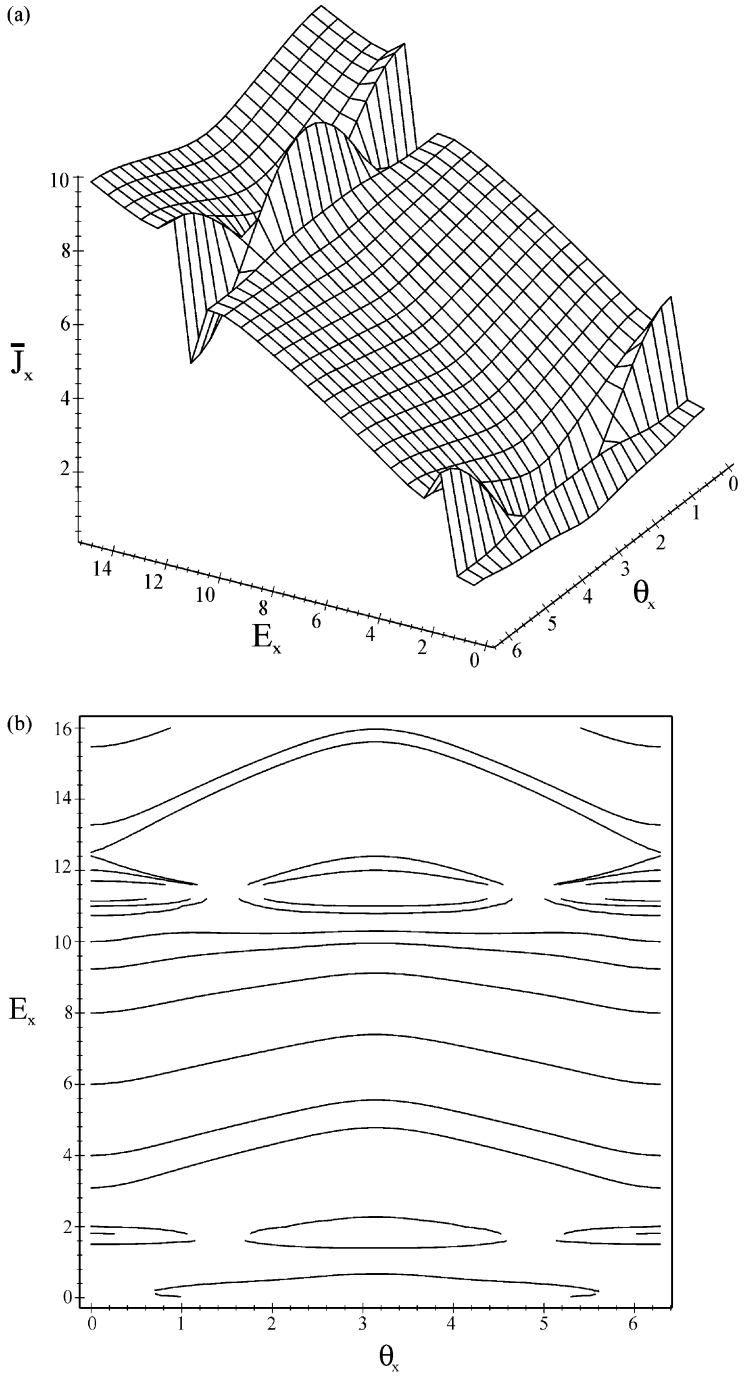

Fig. 4. (a) The function $\bar{J}_x = \bar{J}_x(E_x, \theta_x)$ and (b) the corresponding (E_x, θ_x)-surface of section with the $(\omega_x = \omega_y)$-resonance, for at $\varepsilon = 10^{-1}$ and $E_y = 10^{-2}$. The areas around $E_x = 1.7$ and 11.4 are highly affected by the y-wave through a $(\omega_x = 3\omega_y)$- and $(\omega_x = 5\omega_y)$-resonance, respectively.

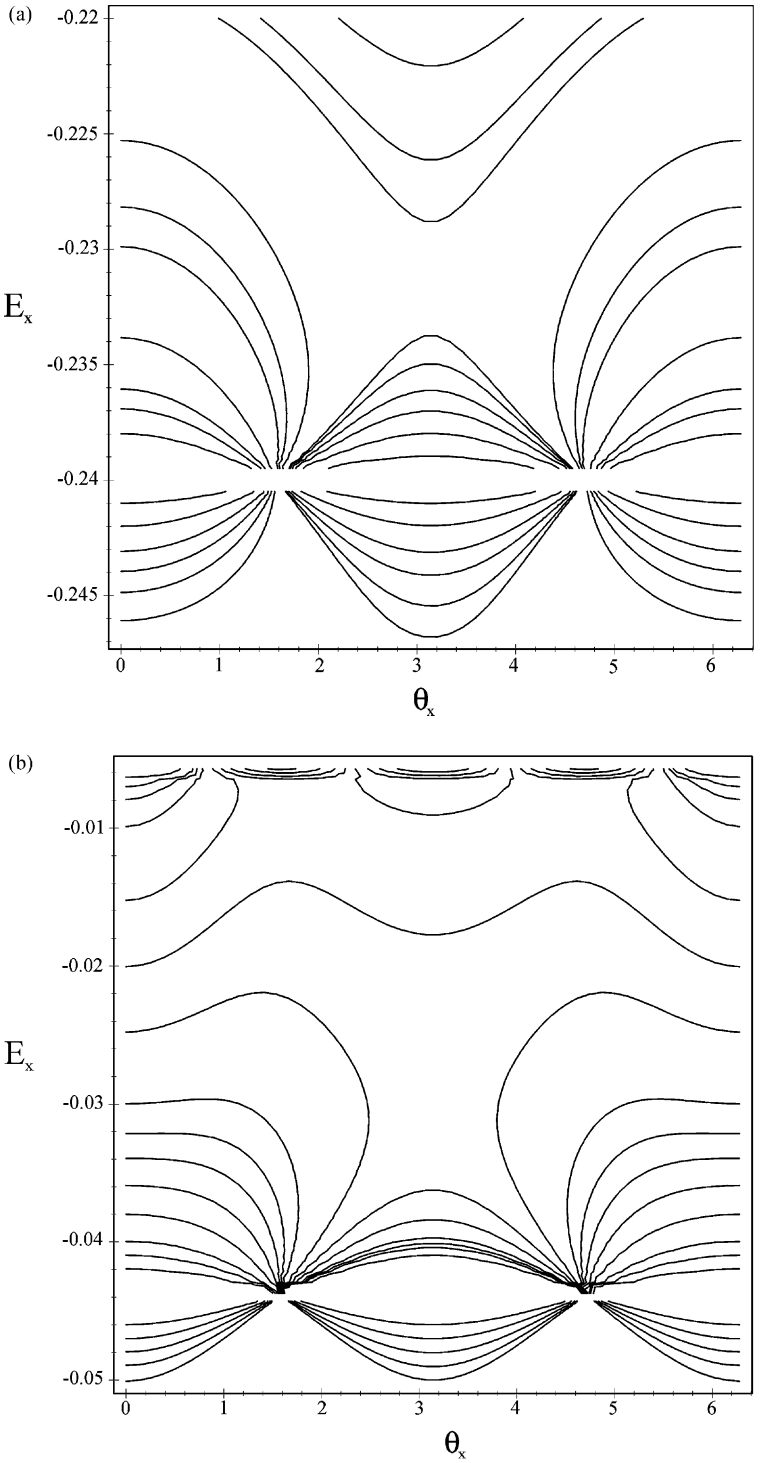

Fig. 5. (a) The (E_x, θ_x)-surface of section in the case of an x-wave coupled with an almost-harmonic y-wave with $E_y = -0.24$. (b) The (E_x, θ_x)-surface of section in the case of an x-wave coupled with a nonharmonic y-wave with $E_y = 10^{-4}$. Here $\varepsilon = 10^{-2}$, while the values $E_x = -0.044$ and -0.005 correspond to $(\omega_x = 2\omega_y)$- and $(2\omega_x = 3\omega_y)$-resonance, respectively.

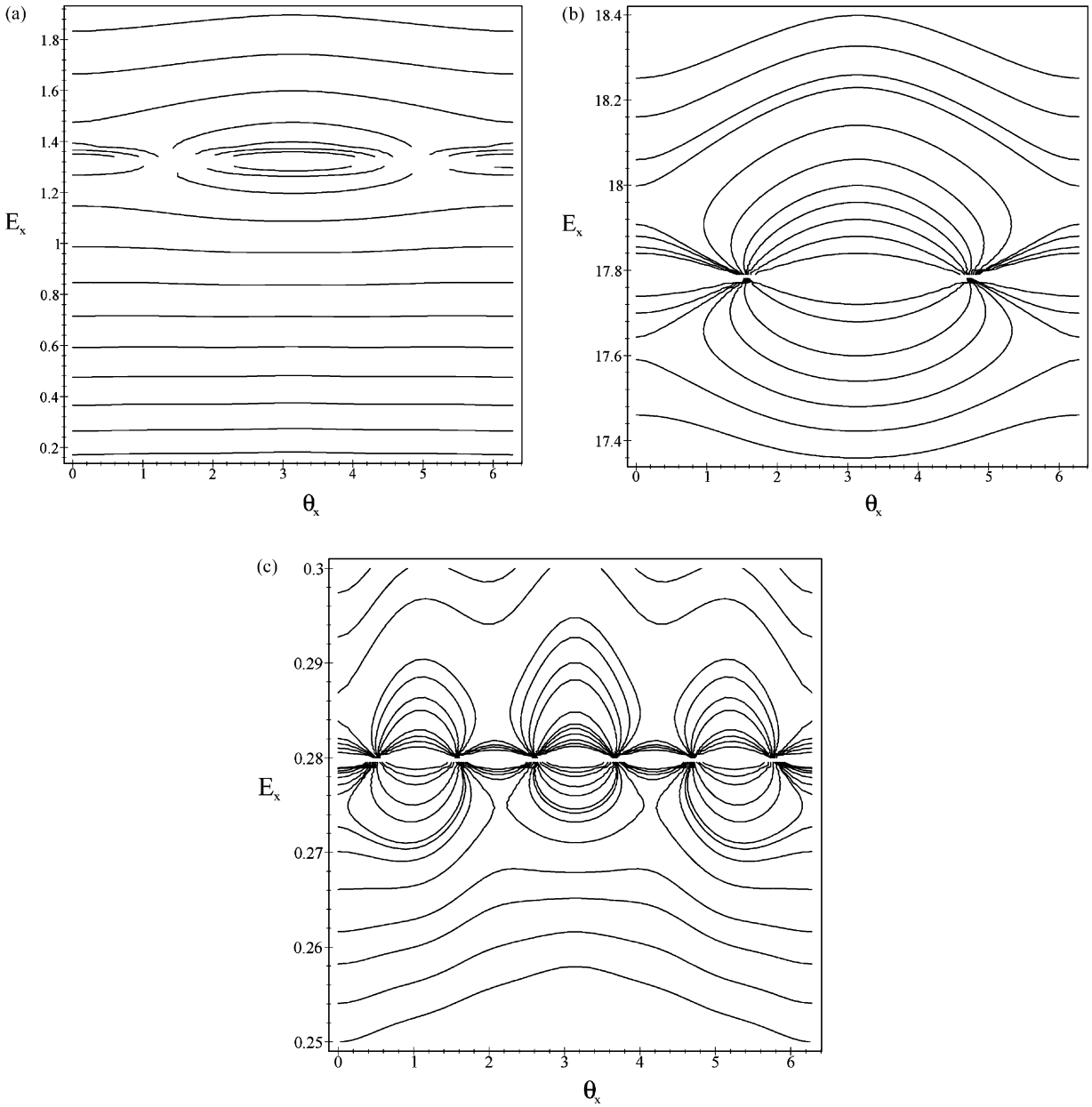

Fig. 6. The (E_x, θ_x)-surfaces in the case of coupling with a y-wave of energy $E_y = -0.1$ with an x-wave of energy: (a) $E_x = 1.32$ at $(\omega_x = \omega_y)$-resonance; (b) $E_x = 17.78$ at $(\omega_x = 2\omega_y)$-resonance; (c) $E_x = 0.28$ at $(3\omega_x = 2\omega_y)$. The coupling strength is $\varepsilon = 10^{-2}$.

where

$$H_{n_x,n_y}(J_x(E_x), J_y(E_y)) = \begin{cases} \frac{1}{2}F_c(E_x, E_y)A_{n_x}(E_x), & n_x > 0, n_y = 0, \\ F_c(E_x, E_y)A_{n_x}(E_x)A_{n_y}(E_y), & n_x > 0, n_y > 0, \end{cases} \tag{37}$$

$$F_c(E_x, E_y) = \sqrt{(1+\sqrt{1+4E_x})(1+\sqrt{1+4E_y})}\,\frac{\pi^2}{2r_x K(r_x)K(q_y)}, \tag{38}$$

$$A_{n_x}(E_x) = \operatorname{sech}\left[\left(n_x - \frac{1}{2}\right)\pi\frac{K'(r_x)}{K(r_x)}\right], \tag{39}$$

$$A_{n_y}(E_y) = \operatorname{sech}\left(n_y\pi\frac{K'(q_y)}{K(q_y)}\right). \tag{40}$$

The first order frequency change due to coupling is, as in Case A

$$\Delta\omega_x = \Delta\omega_y = 0. \tag{41}$$

The two constants of the motion (to first order) are shown in Appendix B. The case where the strength of the coupling is $\varepsilon = 10^{-2}$ and the generalized energy of the y-wave is $E_y = -0.1$ is shown in Fig. 6. The regions on a (E_x, θ_x)-surface of section around the $(\omega_x = \omega_y)$-resonance at $E_x = 1.32$, the $(\omega_x = 2\omega_y)$-resonance at $E_x = 17.78$ and, finally, the $(3\omega_x = 2\omega_y)$-resonance at $E_x = 0.28$, are respectively shown in Fig. 6a–c.

3.2. Resonant interaction

In the vicinity of a resonance in the unperturbed system

$$\frac{\omega_y}{\omega_x} = \frac{r}{s}, \tag{42}$$

where r, s are integers, a resonant denominator appears in the first order invariants calculated in the previous section manifesting a drastic change in the phase space topology of the perturbed system compared to the unperturbed one. The resonant denominators can be eliminated by a canonical transformation to a frame of reference that rotates with the resonant frequency where one of the new angles measures the slow deviation from resonance [17]. Since one can distinguishes between slow and fast angle variables in the transformed system, one may easily average over the fast angle as shown in Appendix C. Then the island width of each resonance can be obtained:

$$\Delta J_{x,\max} = 2\left|\frac{2\varepsilon H_{r,-s}(\mathbf{J}_0)}{\partial^2 H_0/\partial J_{x0}^2}\right|^{1/2}, \tag{43}$$

where J_{x0} is the resonant action. Since J_x is related to the generalized energy E_x of the x-motion, Eq. (43) provides a measure of the energy exchange between the two degrees of freedom near each resonance, a result that is already implied by the first order invariants computed in the previous section. Also, Eq. (43) serves as a good estimate for categorizing the resonances as more and less strong. Furthermore, one may still compute the right hand side of Eq. (43) in terms of resonant generalized energies instead of resonant actions when necessary.

4. Destruction of regular nonlinear periodic waves and transition to chaos

Stochastic instability develops whenever separatrices of neighboring islands overlap [17]. The overlap condition is given in terms of the parameter s

$$s = \frac{1}{2}\frac{\Delta J_{mn} + \Delta J_{m'n'}}{\delta J_{mn}}, \tag{44}$$

where m, n and m', n' are the mode numbers for neighboring resonances and δJ_{mn} is the distance between the resonant actions

$$\delta J_{mn} = |J_{mn} - J_{m'n'}|. \tag{45}$$

The overlap condition states that the majority of the invariant curves obtained in Section 3.1 will be destroyed for $s > 1$ in the region between the two islands considered. The actual structure of invariant surfaces in the transition region $0.7 \leq s \leq 1.5$ can be quite complicated. In terms of the frequency, the parameter s is given as

$$s = \frac{1}{2}\frac{(\mathrm{d}\omega/\mathrm{d}J\,\Delta J)_{mn} + (\mathrm{d}\omega/\mathrm{d}J\,\Delta J)_{m'n'}}{\delta\omega_{mn}}. \tag{46}$$

At this point it is important to specify the meaning of the term 'neighboring resonances', since in frequency ω-space we can find resonances arbitrarily close to a given resonance $\omega_x = (n/m)\omega_y$ (as close as two rational numbers can be). The key thing is the harmonic content of the unperturbed waves, which also determines the width of each resonance. As we have seen, not all the harmonics of the unperturbed waves are significant, so we can distinguish between primary, secondary and higher order resonances.

When the y-wave is almost linear ($E_y >> 0$ for cnoidal waves or $E_y \cong -0.25$ for dnoidal ones) only the first Fourier coefficient is significant so that the resonance condition becomes

$$m\omega_x = \omega_y, \qquad m = 1, 2, \ldots . \tag{47}$$

The sub-harmonic resonances are ordered as follows:

$$\left(\frac{\omega_y}{m}, \frac{\omega_y}{m-1}, \ldots, \frac{\omega_y}{2}, \omega_y\right), \tag{48}$$

while the distance between them is

$$\delta\omega_x = \frac{\omega_y}{m(m+1)} = \frac{\omega_x}{m+1}. \tag{49}$$

If the x-wave is also almost linear ($m = 1$) only one resonance is present and there are no chaotic regions. For large m ($m \gg 1$) the resonances are very close to each other ($\delta\omega_x \to 0$) and the resonant frequency quite small ($\omega_x \to 0$) resulting in a significant Fourier coefficient and a nonnegligible resonance width. As a consequence, resonance overlap takes place near the separatrix even for very small perturbation strength, and there is a stochastic layer in the vicinity of the separatrix the width of which will be determined in the next section in terms of the Melnikov's function.

In the more generic case at which the y-wave is nonlinear the resonant condition is

$$m\omega_x = n\omega_y, \quad m = 1, 2, \ldots, \quad n = 1, 2, \ldots, \tag{50}$$

and we have sub-harmonic ($m > 1, n = 1$), ultra-harmonic ($m = 1, n > 1$) and ultra-sub-harmonic ($n > 1, m > 1$) resonances. The distance between neighboring resonances is

$$\delta\omega_x = \min_{\alpha,\beta} |\omega_{m\pm\alpha,n\pm\beta} - \omega_{m,n}|, \tag{51}$$

where $\alpha = 0, 1$ $\beta = 0, 1$. The overlap condition is obtained after substituting in Eq. (46) the distance between the neighboring resonances and their corresponding widths. When one or both of the interacting waves have large period, resonances between high harmonics have significant width and their centers are very close so they overlap to form a stochastic layer, the width of which is the subject of the next section.

5. Interaction between solitary and nonlinear periodic waves

As we have seen in the previous section when the form of an x-wave approaches the separatrix form ($E_x \to 0$, $\omega_x \to 0$) the resonances with $m \gg 1$ are very close and possess significant widths resulting in resonance overlap in the vicinity of the separatrix. The width of this vicinity can be determined using Melnikov's method for perturbed homoclinic orbits [18–20]. The separatrix solution for the unperturbed system is

$$(x_0(t), \dot{x}_0(t)) = (\pm\sqrt{2}\operatorname{sec} h(t), \mp\sqrt{2}\operatorname{sec} h(t)\tan h(t)), \tag{52}$$

and the Melnikov's integral

$$M(t_0) = \int_{-\infty}^{\infty} \dot{x}_0(t) y(t; t_0)\, \mathrm{d}t, \tag{53}$$

where $y(t;t_0)$ is the unperturbed cnoidal or dnoidal nonlinear periodic solution and t_0 parameterizes the Poincare surface of section on which the x-motion is observed or, equivalently, a specific point on the unperturbed separatrix on a fixed Poincare surface of section.

In the unperturbed system the stable and unstable manifolds of the hyperbolic fixed point (0,0) are joined smoothly to form the separatrix; under perturbation the separatrix splits, the two manifolds intersect transversely and the motion in the vicinity of the unperturbed separatrix is so complicated that is considered as stochastic. Melnikov's integral is related to the distance, d, between the stable and unstable manifolds and its maximum value is a measure of the separatrix splitting and the width of the stochastic layer:

$$d(t_0, \varepsilon; E_y) = \varepsilon \frac{M(t_0; E_y)}{||DH_{0x}(x_0(-t_0), \dot{x}_0(-t_0))||} + O(\varepsilon^2),$$

$$||DH_{0x}(x_0(-t_0), \dot{x}_0(-t_0))|| = \sqrt{\left(\frac{\partial H_{0x}}{\partial x}(x_0(-t_0), \dot{x}_0(-t_0))\right)^2 + \left(\frac{\partial H_{0x}}{\partial \dot{x}}(x_0(-t_0), \dot{x}_0(-t_0))\right)^2}. \tag{54}$$

The distance between the stable and unstable manifold increases at infinity as $t_0 \to \infty$, implying the well-known result of high stochasticity near the hyperbolic fixed point (0,0). For the case of coupling with a cnoidal wave one obtains

$$M(t_{0y}; E_y) = \pm 2\pi\omega_y^2 \sum_{n=1}^{\infty} (2n-1) \operatorname{sec} h\left[\left(n-\frac{1}{2}\right)\pi\frac{K'(r_y)}{K(r_y)}\right] \operatorname{sec} h\left[\left(n-\frac{1}{2}\right)\pi\omega_y\right] \sin\left[\left(n-\frac{1}{2}\right)2\omega_y t_{0y}\right], \tag{55}$$

where the parameter E_y ($E_y > 0$) specifies the member of the one-parameter family of the cnoidal waves. The Melnikov function for the case of coupling with a cnoidal wave is periodic with period which increases exponentially and amplitude that decreases until get almost constant, as E_y approaches zero, as shown in Fig. 7a.

On the other hand, for the case of coupling with a dnoidal wave one obtains

$$M(t_{0y}; E_y) = \pm\pi\omega_y^2 \sum_{n=1}^{\infty} n \operatorname{sec} h\left[n\pi\frac{K'(q_y)}{K(q_y)}\right] \operatorname{sec} h\left[n\frac{\pi\omega_y}{2}\right] \sin[n\omega_y t_{0y}], \tag{56}$$

where now the parameter E_y ($-1/4 < E_y < 0$) parameterizes the members of the one-parameter family of the dnoidal waves. The Melnikov function for this case is shown in Fig. 7b. As in the previous case, the period increases exponentially as E_y approaches zero. However, the amplitude increases until gets almost constant.

For both of cases the Melnikov function tends to be nonperiodic as E_y approaches zero, that is, the nonlinear periodic y-wave approaches the form of the solitary pulse corresponding to the separatrix. It is shown in Fig. 7c.

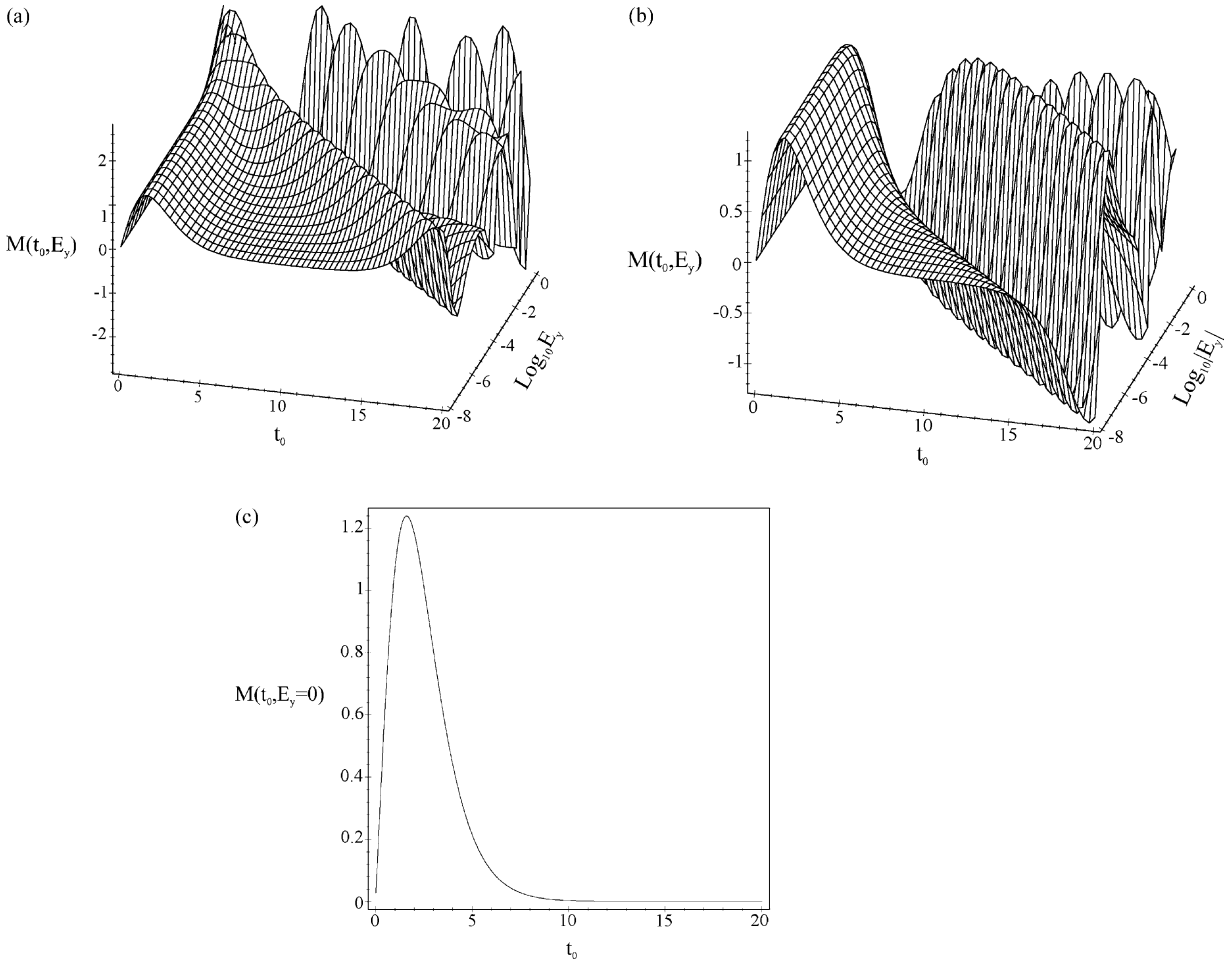

Fig. 7. The Melnikov function for the case of coupling with a: (a) cnoidal wave; (b) dnoidal wave; (c) a nonlinear periodic *y*-wave approaching the form of a solitary pulse.

6. Conclusions

In conclusion, in this work we studied the traveling-wave solutions dynamics of two linearly coupled NLSEs, describing the wave propagation in a dual-core fiber. Interactions between both nonlinear periodic waves and solitary pulses were considered. Nonlinear periodic waves correspond to periodic trains of pulses and in the limiting case of an infinite period they transform to almost ideal solitons. In fact, in fiber transmission lines as well as in any component of an optical network, one deals not purely with localized solitons but with the trains of such pulses. Although, the time separation between these pulses is not constant consideration of nonlinear periodic waves enables to shed some light on the behavior of optical pulses in more complex trains. In order to study, not only switching properties, but the full range of functionality as well, of a two-port device (such as an optical coupler) we consider the general case of having two inputs and investigate resonant interactions of two channels, one of which can play the role of a control signal.

The interaction of nonlinear periodic waves was studied, using canonical perturbation theory. The surface of section of the phase space that corresponds to each wave is obtained as a contour plot of an approximate invariant of the system. It was shown that the presence of a nonlinear periodic wave of a given frequency in one of the cores distorts a wave on the other core through parametric resonance. The two waves exchange energies periodically. The amount of the energy that is transferred from one wave to another depends on the frequency and, consequently, on the amplitude of the waves. It is larger for waves with frequencies that are close to satisfy a resonance relation. As a result, the phase space distortion due to interaction is not uniform and there are regions of weak, strong and even chaotic interactions, depending also on the interaction strength, which is the small parameter in the perturbation method used. The coupling strength threshold above which the interaction between two nonlinear waves of given amplitude becomes chaotic (and destruction of regular waves occur) was also estimated.

The interaction of a solitary pulse with a nonlinear periodic wave (cnoidal or dnoidal wave) was studied using the Melnikov method for homoclinic orbits. This interaction causes stochastization of the homoclinic orbit, which corresponds to the solitary pulse. The separatrix splitting and the width of the stochastic layer near the homoclinic orbit was given in terms of the Melnikov function for the two kinds of the nonlinear waves considered. On the other hand, the interaction of two solitary pulses can be seen as the limiting case of a nonlinear periodic wave with large period tending to infinity, that is, approaching the pulse shape which corresponds to the homoclinic orbit (namely the hyperbolic secant profile).

Acknowledgements

The authors are indebted to the late Professor C. Polymilis for useful discussions. This work has been supported in part by the Archimedes Grant of the Institute of Communications and Computer Systems/National Technical University of Athens and in part by the General Secretariat of Research and Development under Contract No. PENED-95/644.

Appendix A

For the case $q > 0$, which is the most relevant for the dual-core fiber system, the model is equivalent with that of a particle moving in the double well potential

$$V(x) = -\frac{x^2}{2} + \frac{x^4}{4}. \tag{A.1}$$

There are three kinds of motion allowed by $V(x)$ depending on the value of the (constant) energy of the oscillator

$$E_x = H_{0x}(x, \dot{x}). \tag{A.2}$$

If $E_x > 0$ one easily obtains the nonlinear periodic solution

$$x(t) = \pm\sqrt{1 + \sqrt{1 + 4E_x}}\, cn(\sqrt[4]{1 + 4E_x}\, t + t_0), \tag{A.3}$$

with period

$$T = \frac{4K(r)}{(1 + 4Ex)^{1/4}}, \qquad r = \frac{\sqrt{1 + \sqrt{1 + 4E_x}}}{\sqrt{2}\sqrt[4]{1 + 4E_x}}, \tag{A.4}$$

while for $-1/4 \leq E_x < 0$ the nonlinear periodic solution assumes the following form:

$$x(t) = \pm\sqrt{1+\sqrt{1+4E_x}}\,dn\left(\frac{\sqrt{1+\sqrt{1+4E_x}}}{\sqrt{2}}t + t_0\right), \tag{A.5}$$

with period

$$T = \frac{2\sqrt{2}K(q)}{\sqrt{1+\sqrt{1+4E_x}}}, \qquad q = \frac{\sqrt{2}\sqrt[4]{1+4E_x}}{\sqrt{1+\sqrt{1+4E_x}}}. \tag{A.6}$$

Here *cn* and *dn* are the Jacobi elliptic functions and $K(\cdot)$ is the complete elliptic integral of the first kind.

Near the separatrix ($E \to 0$) the period is given by $T(E_x) = l\ln(16/|E_x|) + O(E_x)$ with $l = 1$ for $E_x < 0$ and $l = 2$ for $E_x > 0$. For $E_x = 0$ one obtains the asymptotic solution

$$x(t) = \pm\sqrt{2}\,\mathrm{sec}\,h(t + t_0), \tag{A.7}$$

corresponding to a solitary wave of the NLSE.

The transformation of the unperturbed system to action-angle variables (J, θ) is

$$J_x(E_x) = \frac{2}{3\pi}\sqrt[4]{1+4E_x}[(-1+\sqrt{1+4E_x})K(r) - 4E(r)] \quad \text{for } E_x > 0, \tag{A.8}$$

$$J_x(E_x) = \frac{\sqrt{2}}{6\pi}\sqrt{1+\sqrt{1+4E_x}}[2E(q) - 2(1-\sqrt{1+4E_x})K(q)] \quad \text{for } -\frac{1}{4} \leq E_x < 0, \tag{A.9}$$

$$x = \sqrt{1+\sqrt{1+4E_x}}\,cn\left(\frac{2K(r)}{\pi}\theta\right) \quad \text{for } E_x > 0, \tag{A.10}$$

$$x = \sqrt{1+\sqrt{1+4E_x}}\,dn\left(\frac{K(q)}{\pi}\theta\right) \quad \text{for } -\frac{1}{4} \leq E_x < 0. \tag{A.11}$$

The action-angle variables are defined only for periodic motions, so the transformation is not defined for $E_x = 0$ (asymptotic solution).

In Fourier series the periodic solutions are expressed as follows:

$$x = \pm\sqrt{1+\sqrt{1+4Ex}}\,\frac{\pi}{rK(r)}\sum_{n=1}^{\infty}\mathrm{sec}\,h\left[\left(n-\frac{1}{2}\right)\pi\frac{K'(r)}{K(r)}\right]\cos[(2n-1)\theta], \qquad E_x > 0, \tag{A.12}$$

$$x = \pm\sqrt{1+\sqrt{1+4Ex}}\,\frac{\pi}{K(q)}\left\{\frac{1}{2} + \sum_{n=1}^{\infty}\mathrm{sec}\,h\left(n\pi\frac{K'(q)}{K(q)}\right)\cos(n\theta)\right\}, \qquad -\frac{1}{4} \leq E_x < 0, \tag{A.13}$$

where $K'(\cdot)$ is the complementary elliptic integral of the first kind and r, q are defined as in Eqs. (A.4) and (A.6), respectively.

Finally, the case $q < 0$ corresponds to a single well potential with only one minimum at zero, oscillating solutions given in terms of Jacobi *sd* functions and no asymptotic solution is present.

Appendix B

The approximate constants of the motion (to first order) for the three cases are:

Case A.

$$J_x(E_x) + \varepsilon \sum_{n_x,n_y=1}^{\infty} H_{n_x,n_{yx}}(E_x, E_y)(2n_x - 1) \times \left\{ \frac{\cos[(2n_x - 1)\theta_\chi + (2n_y - 1)\theta_y]}{(2n_x - 1)\omega_\chi + (2n_y - 1)\omega_y} + \frac{\cos[(2n_x - 1)\theta_\chi - (2n_y - 1)\theta_y]}{(2n_x - 1)\omega_\chi - (2n_y - 1)\omega_y} \right\},$$

$$J_y(E_y) + \varepsilon \sum_{n_x,n_y=1}^{\infty} H_{n_x,n_y}(E_x, E_y)(2n_y - 1) \times \left\{ \frac{\cos[(2n_x - 1)\theta_\chi + (2n_y - 1)\theta_y]}{(2n_x - 1)\omega_\chi + (2n_y - 1)\omega_y} - \frac{\cos[(2n_x - 1)\theta_\chi - (2n_y - 1)\theta_y]}{(2n_x - 1)\omega_\chi - (2n_y - 1)\omega_y} \right\}, \tag{B.1}$$

Case B.

$$J_x(E_x) + \varepsilon \sum_{n_x=1,n_y=0}^{\infty} H_{n_x,n_y}(E_x, E_y) n_x \left[\frac{\cos(n_x\theta_x + n_y\theta_y)}{n_x\omega_x + n_y\omega_y} + \frac{\cos(n_x\theta_x - n_y\theta_y)}{n_x\omega_x - n_y\omega_y} \right],$$

$$J_y(E_y) + \varepsilon \sum_{n_x=0,n_x=1}^{\infty} H_{n_x}(E_x, E_y) n_y \left[\frac{\cos(n_x\theta_x + n_y\theta_y)}{n_x\omega_x + n_y\omega_y} - \frac{\cos(n_x\theta_x - n_y\theta_y)}{n_x\omega_x - n_y\omega_y} \right], \tag{B.2}$$

Case C.

$$J_x(E_x) + \varepsilon \sum_{n_x=1,n_y=0}^{\infty} H_{n_x,n_y}(E_x, E_y)(2n_x - 1) \left[\frac{\cos((2n_x - 1)\theta_x + n_y\theta_y)}{(2n_x - 1)\omega_x + n_y\omega_y} + \frac{\cos((2n_x - 1)\theta_x - n_y\theta_y)}{(2n_x - 1)\omega_x - n_y\omega_y} \right],$$

$$J_y(E_y) + \varepsilon \sum_{n_x,n_y=1}^{\infty} H_{n_x,n_y}(E_x, E_y) n_y \left[\frac{\cos((2n_x - 1)\theta_x + n_y\theta_y)}{(2n_x - 1)\omega_x + n_y\omega_y} - \frac{\cos((2n_x - 1)\theta_x - n_y\theta_y)}{(2n_x - 1)\omega_x - n_y\omega_y} \right]. \tag{B.3}$$

Appendix C

The generating function

$$F_2 = (r\theta_x - s\theta_y)\hat{J}_x + \theta_y \hat{J}_y, \tag{C.1}$$

defines the canonical transformation

$$J_x = r\hat{J}_x, \qquad J_y = \hat{J}_y - s\hat{J}_x, \qquad \hat{\theta}_x = r\theta_x - s\theta_y, \qquad \hat{\theta}_y = \theta_y. \tag{C.2}$$

This transformation is equivalent to observing the motion in a rotating frame in which the rate of change of the new variable

$$\dot{\hat{\theta}}_x = r\dot{\theta}_x - s\dot{\theta}_y, \tag{C.3}$$

measures the slow deviation from resonance. Applying (C.2) to the Hamiltonian

$$H = H_0(\mathbf{J}) + \varepsilon H_1(\mathbf{J}, \boldsymbol{\theta}), \qquad H_1 = \sum_{n_x,n_y} H_{n_x,n_y}(\mathbf{J}) \exp(i\mathbf{m} \cdot \boldsymbol{\theta}), \qquad \mathbf{m} = (n_x, n_y), \tag{C.4}$$

one obtains

$$\hat{H} = \hat{H}_0(\hat{\mathbf{J}}) + \varepsilon \hat{H}_1(\hat{\mathbf{J}}, \hat{\theta}), \tag{C.5}$$

where

$$\hat{H}_1 = \sum_{n_x, n_y} H_{n_x, n_y}(\hat{\mathbf{J}}) \exp\left\{ \frac{i}{r}[n_x \hat{\theta}_x + (n_x s + n_y r)\hat{\theta}_y] \right\}. \tag{C.6}$$

Averaging over the fast angle $\hat{\theta}_y$ yields

$$\bar{H} = \bar{H}_0(\hat{\mathbf{J}}) + \varepsilon \bar{H}_1(\hat{\mathbf{J}}, \hat{\boldsymbol{\theta}}_x), \tag{C.7}$$

where

$$\bar{H}_0 = \hat{H}_0(\hat{\mathbf{J}}), \tag{C.8}$$

and

$$\bar{H}_1 = \left\langle \hat{H}_1(\hat{\mathbf{J}}, \hat{\boldsymbol{\theta}}) \right\rangle_{\hat{\theta}_2} = \sum_{p=0}^{\infty} H_{-pr,ps}(\hat{\mathbf{J}}) \exp(-ip\hat{\mathbf{J}}_1), \tag{C.9}$$

which defines a system of effectively one-degree of freedom in $(\hat{J}_x, \hat{\theta}_x)$ since

$$\dot{\hat{J}}_y = \frac{\partial \bar{H}}{\partial \hat{\theta}_y} = 0 \text{ and } \hat{J}_y = \text{constant}. \tag{C.10}$$

The $(\hat{J}_x, \hat{\theta}_x)$-motion can be described to a good approximation if one keeps only the $p = 0, \pm 1$ terms, since $H_{-pr,ps}$ fall rapidly as p increases. This truncated system has two fixed points one being stable (elliptic) and the other unstable (hyperbolic). Simple analysis leads to an estimate for the maximum excursion of the action from the stable fixed point

$$\Delta \hat{J}_{x,\max} = 2 \left| \frac{2\varepsilon H_{r,-s}(\hat{\mathbf{J}}_0)}{\partial^2 \hat{H}_0 / \partial \hat{J}_{x0}^2} \right|^{1/2} = O[(\varepsilon H_{r,-s})^{1/2}], \tag{C.11}$$

where $\hat{J}_{x0}$ is the action at the elliptic fixed point.

References

[1] S.M. Jensen, IEEE J. Quant. Electron. QE-18 (1982) 1580.
[2] M. Romagnoli, S. Trillo, S. Wabnitz, Opt. Quant. Electron. 24 (1992) S1237.
[3] S.L. Doty, J.W. Haus, Y.J. Oh, R.L. Fork, Phys. Rev. E 51 (1995) 709.
[4] Y.S. Kivshar, Opt. Lett. 18 (1993) 7.
[5] B.A. Umarov, F.Kh. Abdullaev, M.R.B. Wahiddin, Opt. Commun. 162 (1999) 340.
[6] S. Wabnitz, E.M. Wright, C.T. Seaton, G.I. Stegeman, Appl. Phys. Lett. 49 (1986) 838.
[7] H. Hatami-Hanza, P.L. Chu, Opt. Commun. 124 (1996) 90.
[8] P. Shum, K.S. Chiang, W.A. Gambling, IEEE J. Quant. Electron. 35 (1999) 79.
[9] G.D. Peng, B.A. Malomed, P.L. Chu, Phys. Scr. 58 (1998) 149.
[10] P.L. Chu, Y.S. Kivshar, B.A. Malomed, G.D. Peng, M.L. Quiroga-Teixeiro, JOSA B12 (1995) 898.
[11] A.V. Buryak, N.N. Akhmediev, Opt. Commun. 110 (1994) 287.
[12] A. Mostofi, B.A. Malomed, P.L. Chu, Opt. Commun. 145 (1998) 274.
[13] N.N. Akhmediev, A. Ankiewicz, Solitons: Nonlinear Pulses and Beams, Chapman & Hall, London, 1997.
[14] B.M. Herbst, M.J. Ablowitz, Phys. Rev. Lett. 62 (1989) 2065.

[15] N.N. Akhmediev, A. Ankiewicz, Phys. Rev. Lett. 70 (1993) 2395.
[16] A.J. Lichtenberg, M.A. Lieberman, Regular and Stochastic Motion, Springer, New York, 1983.
[17] B.V. Chirikov, Phys. Rep. 52 (1979) 263.
[18] J. Guckenheimer, P. Holmes, Nonlinear Oscillations, Dynamical Systems and Bifurcations of Vector Fields, Springer, New York, 1983.
[19] S. Wiggins, Introduction to Applied Nonlinear Dynamical Systems and Chaos, Springer, New York, 1990.
[20] G.M. Zaslavsky, Chaos 4 (1994) 3.